The Astrophysical Journal Letters, 780:L27 (6pp), 2014 January 10 doi:10.1088/2041-8205/780/2/L27

FERMI RULES OUT THE INVERSE COMPTON/CMB MODEL FOR THE LARGE-SCALE JET X-RAY EMISSION OF 3C 273

Eileen T. Meyer[1,2] and Markos Georganopoulos[2,3]
[1] Space Telescope Science Institute, 3700 San Martin Drive, Baltimore, MD 21218, USA
[2] Department of Physics, University of Maryland Baltimore County, 1000 Hilltop Circle, Baltimore, MD 21250, USA
[3] NASA Goddard Space Flight Center, Code 660, Greenbelt, MD 20771, USA
Received 2013 July 30; accepted 2013 November 27; published 2013 December 17

ABSTRACT

The X-ray emission mechanism in large-scale jets of powerful radio quasars has been a source of debate in recent years, with two competing interpretations: either the X-rays are of synchrotron origin, arising from a different electron energy distribution than that producing the radio to optical synchrotron component, or they are due to inverse Compton scattering of cosmic microwave background photons (IC/CMB) by relativistic electrons in a powerful relativistic jet with bulk Lorentz factor $\Gamma \sim 10$–20. These two models imply radically different conditions in the large-scale jet in terms of jet speed, kinetic power, and maximum energy of the particle acceleration mechanism, with important implications for the impact of the jet on the large-scale environment. A large part of the X-ray origin debate has centered on the well-studied source 3C 273. Here we present new observations from *Fermi* which put an upper limit on the gamma-ray flux from the large-scale jet of 3C 273 that violates at a confidence greater that 99.9% the flux expected from the IC/CMB X-ray model found by extrapolation of the UV to X-ray spectrum of knot A, thus ruling out the IC/CMB interpretation entirely for this source when combined with previous work. Further, this upper limit from *Fermi* puts a limit on the Doppler beaming factor of at least $\delta < 9$, assuming equipartition fields, and possibly as low as $\delta < 5$, assuming no major deceleration of the jet from knots A through D1.

Key words: galaxies: active – galaxies: jets – quasars: individual (3C 273) – radiation mechanisms: non-thermal

Online-only material: color figure

1. INTRODUCTION

Large-scale jets (LSJs) of kpc–Mpc size have been observed in radio images of radio-loud active galactic nuclei (AGNs) almost since their discovery, but only more recently has high-resolution imaging with the *Hubble Space Telescope* (*HST*) and the *Chandra X-Ray Observatory* shown that the knots in many of these LSJs often produce significant high-energy radiation. Since the first (serendipitous) *Chandra* detection of a large-scale X-ray jet in PKS 0637-752 (Chartas et al. 2000), several dozen have been discovered (see Harris & Krawczynski 2006, for a review), spanning a range from typically lower radio power Fanaroff and Riley (FR; Fanaroff & Riley 1974) type I to more powerful FR II type radio galaxies.

With high-resolution multi-band imaging, we are now able to build reliable spectral energy distributions (SEDs) for the LSJ emission, separate from the blazar core. In many cases, the spectra of the knots appears consistent with a single synchrotron origin from radio to X-rays, as seen in M87 (Wilson & Yang 2002; Perlman & Wilson 2005), B2 0331+39 (Worrall et al. 2001), and 3C 31 (Hardcastle et al. 2002), and several others, all notably FR I sources. However, in several of the more powerful (typically FR II) sources, the X-ray spectrum in the knots is clearly much harder and/or higher than would be consistent with the radio–optical synchrotron spectrum, as first observed by Schwartz et al. (2000) and Chartas et al. (2000) for PKS 0637-752.

Based on that finding, Tavecchio et al. (2000) and Celotti et al. (2001) suggested that the X-rays could be due to inverse Compton scattering of cosmic microwave background photons (IC/CMB) by relativistic electrons in the jet.[4] The IC/CMB model has since been applied to other jets with X-rays inconsistent with their radio–optical synchrotron spectra, including the well-studied source 3C 273 (Sambruna et al. 2001), and many more FR II X-ray jets subsequently discovered (e.g., Sambruna et al. 2004; Worrall 2009; Mehta et al. 2009; see also the "two-zone" IC/CMB model for PKS 1127-145 of Siemiginowska et al. 2007). Generally, the IC/CMB model requires that the jet remain highly relativistic out to the location of the X-ray knots (bulk Lorentz factor $\Gamma \sim 10$–20), point close to our line of sight, and have an electron energy distribution (EED) extending down to energies $\sim$1–10 MeV, significantly lower than the $\sim$1–10 GeV electron energies traced by GHz synchrotron radio emission. To produce the observed X-ray flux, IC/CMB requires high, sometimes super-Eddington jet kinetic power (Dermer & Atoyan 2004; Uchiyama et al. 2006), due to the low radiative efficiency of these electrons. Also, the small angle to the line of sight in several cases requires Mpc-scale de-projected jet lengths, as long as the longest radio galaxies observed (Dermer & Atoyan 2004; Sambruna et al. 2008).

Deep *HST* imaging photometry of the knots in PKS 1136-135 also reveals "improbability" issues with the IC/CMB model, with the observed optical polarization exceeding 30%; applying the IC/CMB model requires a significantly super-Eddington jet longer than a Mpc, forming a $\sim 2\overset{\circ}{.}5$ angle

[4] Synchrotron self-Compton has been shown to be an inadequate mechanism to produce the observed X-ray flux in these sources, unless the magnetic field in the jet is orders of magnitude below the equipartition value (e.g., Chartas et al. 2000).

to the line of sight and having a Doppler beaming factor $\delta > 20$ (Cara et al. 2013).

An alternative explanation for the X-rays in powerful sources is synchrotron emission from an additional EED (e.g. Hardcastle 2006; Jester et al. 2006; Uchiyama et al. 2006). Because the synchrotron emission mechanism is far more efficient than IC/CMB, it does not require the high Lorentz factors, extreme jet lengths or near-Eddington jet powers, as the IC/CMB model does in several cases (Jorstad & Marscher 2004; Uchiyama et al. 2006). However, it is not clear what physical mechanism might produce this second EED, and in some cases the observed SED requires the high-energy particle population to have a difficult-to-explain low-energy cutoff at ∼TeV energies, where fast cooling is unavoidable (Mehta et al. 2009).

One of the best-studied LSJs is seen in the powerful nearby ($z = 0.158$) quasar 3C 273. Imaging in all bands reveals similar features, with a knotty jet beginning about 12″ from the blazar core and extending a further 12″ downstream. Extensive observations with *HST*, *Spitzer*, and *Chandra* have revealed that the knots are characterized by two spectral components, one with a cutoff above 5×10^{13} Hz and a high-energy one connecting the optical–UV and X-ray data (Jester et al. 2005, 2006; Uchiyama et al. 2006). Georganopoulos et al. (2006, hereafter G06), showed that while the radio to X-ray SED of this source alone cannot discriminate between the IC/CMB and synchrotron models, *gamma-ray* observations, specifically with *Fermi*, may be able to do so. As discussed in G06, if the X-rays from the 3C 273 jet are due to IC/CMB, a hard, steady spectrum is also expected in the gamma rays by extension (see also Sambruna et al. 2004). If *Fermi* detects this emission (or puts limits on it) at a level significantly below what is expected by extrapolation from the X-rays, the IC/CMB model for the X-rays will be ruled out.

The competing IC/CMB and synchrotron models imply radically different views of the LSJ power, bulk Lorentz factor, and the efficiency of particle acceleration, resulting in very different impacts on the host galaxy and surrounding environment. The persistently open question of the nature of the X-rays is critical not only for understanding jet physics but also for our understanding of AGN activity as a feedback mechanism in galaxy formation, yet until now no conclusive evidence has arisen to eliminate either model.

In this paper, we analyze the gamma rays of 3C 273 for evidence of the expected hard, flat spectrum from IC/CMB which has been suggested as the source of the X-rays in this and other powerful LSJs. In Section 2, we discuss the method of the *Fermi* data analysis and our finding that no IC/CMB emission has been detected. In Section 3 we discuss the resulting upper limit on the IC/CMB emission along with constraints on the Doppler beaming factor. In Section 4 we derive a limit for the bulk Lorentz factor based on our *Fermi* result.

2. *FERMI* ANALYSIS OF 3C 273

We first computed the light curve of 3C 273 using bins of equal Good Time Interval (GTI) time, totaling 648,000 s (7.5 days) per bin, corresponding to a range of 15–23 days in real time. Using the standard pipeline tools (version v9r27p1) and the latest instrument response function (P7SOURCE_V6), the flux of 3C 273 was calculated using (unbinned) maximum likelihood with the `gtlike` tool. We used a region of interest of 7°; all sources (29) listed in the two-year catalog (2FGL; Nolan et al. 2012) within 15° of the position of 3C 273 were included in the initial model. In some bins, known sources which were undetected were removed in order to gain convergence. 3C 273 was modeled as a simple power law with spectral index and normalization free. When the test statistic (TS; roughly equivalent to significance squared) for 3C 273 was <10, we used the *Fermi* `UpperLimit` tool which uses the profile likelihood method (e.g., Barndorff-Nielsen & Cox 1994), freezing the other source parameters to generate upper limits.

Table 1
Fermi Analysis Results

Energy Bin	Limit	Energy Flux (erg s^{-1} cm^{-2})
100–300 MeV		$1.30 \pm 0.24 \times 10^{-11}$
300–1000 MeV		$8.50 \pm 0.78 \times 10^{-12}$
1–3 GeV		$2.43 \pm 0.62 \times 10^{-12}$
3–10 GeV	95%	$<4.9 \times 10^{-13}$
	99%	$<9.4 \times 10^{-13}$
	99.9%	$<1.6 \times 10^{-12}$
10–100 GeV	95%	$<2.5 \times 10^{-12}$
	99%	$<3.6 \times 10^{-12}$
	99.9%	$<4.9 \times 10^{-12}$

The light curve of 3C 273 from 2008 August 4 to 2013 March 11 (*Fermi* Mission Elapsed Time (MET) 239,557,417–384,684,952 s) is shown in Figure 1, with total flux versus the central MET of the corresponding bin in the upper panel, and TS versus the latter in the lower panel.

Previous calculations (G06) have shown that it may be possible to detect the hard, steady component from IC/CMB by the LSJ when the competing blazar emission is at a minimum. However, the analysis is complicated by the fact that *Fermi* lacks the spatial resolution to resolve the LSJ separately from the blazar core, as the *Fermi* angular resolution ranges from 3.°5 at 100 MeV down to ∼0.°15 above 10 GeV, at which point it is still an order of magnitude larger than the scale of the LSJ. As can be seen from Figure 1, the core appears to dominate the emission, with significant short-term variability with timescales on the order of the bin widths.

In order to gain the increased sensitivity of a longer integration time on the source while avoiding times where the blazar may come "up" during an otherwise quiescent period, we used a progressive binning approach, in which the light-curve bins were ordered by total flux. Beginning with the bin with lowest flux, we then added the next-highest bin (not necessarily contiguous) in succession and re-ran the likelihood analysis for the combined time frame at each addition. The SED was divided into the five "standard" energy ranges used in the 2FGL: 100–300 MeV, 300 MeV-1 GeV, 1–3 GeV, 3–10 GeV, and 10–100 GeV. As above, when a given energy bin found TS < 10, an upper limit was calculated. Overall, the flux calculations behaved as expected: initially all bands were upper limits, which became progressively lower as more time bins were used, up to the point where the blazar was detected, when the flux values began increasing in the lower-energy bins (see Figure 1(c)).

The two highest energy bins (3–10 GeV and 10–100 GeV) gave only upper limit fluxes during the entire analysis, reaching a minimum after the 25 lowest bins were analyzed together. The inclusion of bins after the 25th lowest only increased fluxes (or upper limits) in all energy bands. Therefore we report the 95%, 99%, and 99.9% upper limits on the fluxes in the 3–10 and 10–100 GeV bands in Table 1 using these 25 bins, in addition to the detected total fluxes in the first three bins. We note that the background at energies >3 GeV from nearby sources is very low

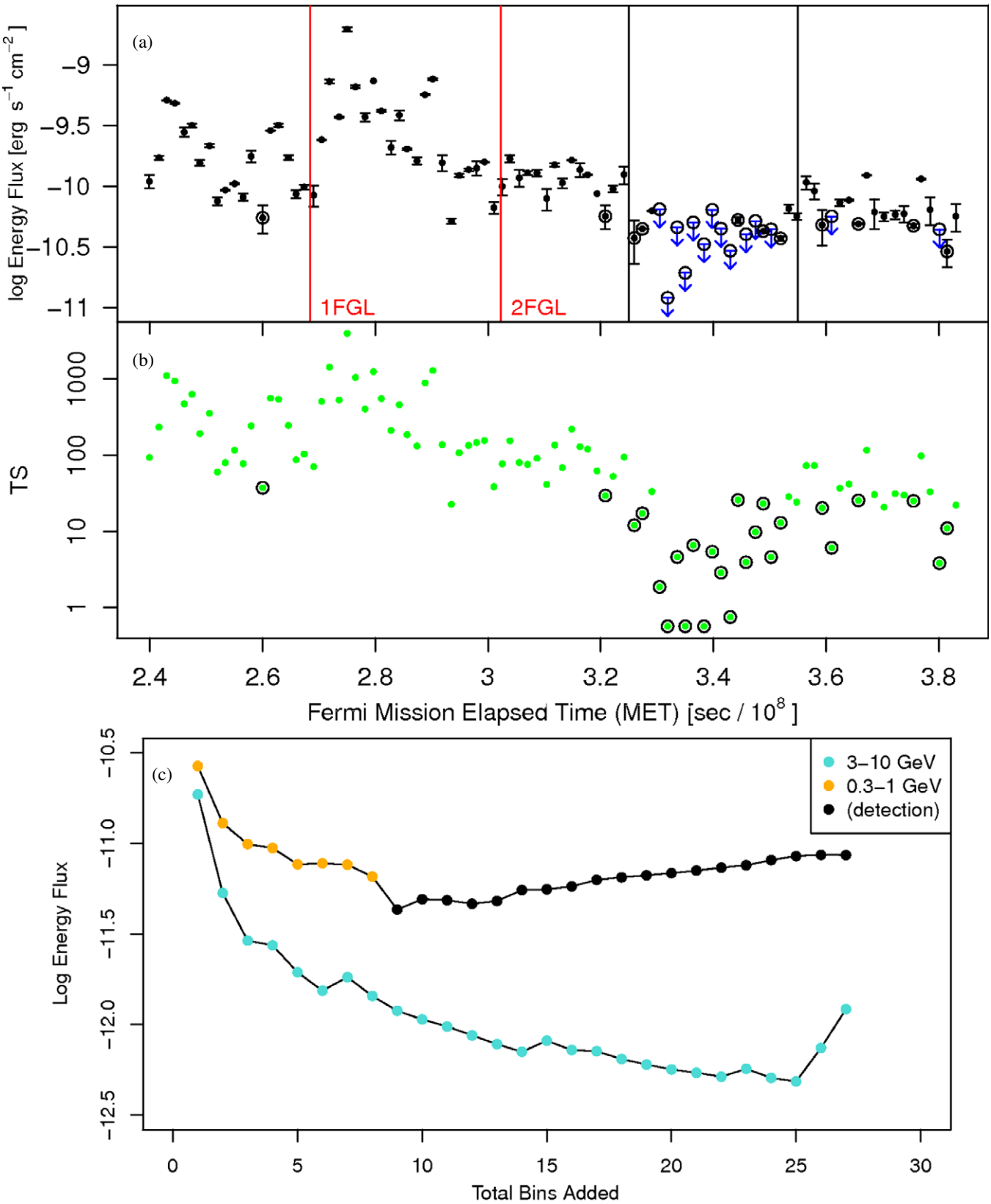

Figure 1. (a) Total light curve of 3C 273 (2008 August 4 to 2013 March 11) in bins of equal GTI time (7.5 days), showing total *Fermi* band (100 MeV to 100 GeV) energy flux vs. MET. The 1FGL and 2FGL catalog end times are noted with red lines. Detections are shown as points with error bars, while upper limits (when the TS of the source was <10) are shown as arrows. The circled points in both panels are the 25 lowest bins which were combined to give the lowest limit on the jet emission. (b) The TS of each bin vs. MET. (c) The flux limit of the 0.3–1 GeV and 3–10 GeV bands with increasing integration time. Colored points indicate upper limits; black are detections.

(A color version of this figure is available in the online journal.)

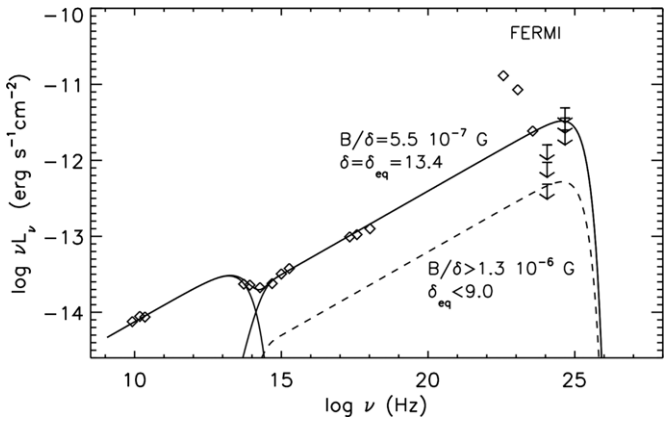

Figure 2. SED of knot A (data from Uchiyama et al. 2006 and Jester et al. 2005, 2006), along with the *Fermi* 95%, 99%, and 99.9% upper limits described in Section 2 and Table 1. The numerical SED calculated at equipartition (solid line) overproduces the 3–10 GeV 99.9% *Fermi* upper limit, ruling out the IC/CMB model for the X-ray emission of knot A. The broken line is the highest level the IC/CMB component can have without violating the 95% 3–10 GeV band *Fermi* upper limit.

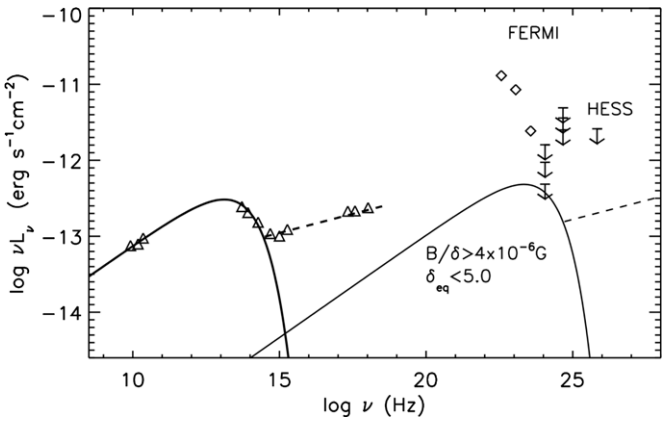

Figure 3. SED of the jet from knot A to knot D1 (data from Uchiyama et al. 2006 and Jester et al. 2005, 2006), including *Fermi* measurements and upper limits described in Section 2, and a HESS upper limit (Aharonian et al. 2005). The thick solid line is a parametric fit of the synchrotron SED following Uchiyama et al. (2006) and G06. The thick broken straight line is the SED of the UV–X-ray component, assumed to be of synchrotron nature. The thin solid line, following the scalings of Equations (1) and (2) is the maximum amplitude the IC/CMB SED produced by the same electrons producing the synchrotron thick solid line SED can have without violating the 3–10 GeV band *Fermi* 95% upper limit. The thin broken line is the IC/CMB SED that results from the same electrons that produce the UV–X-ray synchrotron emission.

as the nearest source (PKS 1217+02) is at a distance of almost five times the 95% containment radius at this energy (∼0.°5).

Alternative methods of ordering the bins are possible (such as strictly on upper limit flux value, or by TS); these methods give practically identical results (nearly the same ordering and a minimum flux in the final two bins within a few percent of the above values). The final five-band SED points are shown in Figures 2 and 3. It is clear that the first three bins are a representation of the low-level blazar SED, which is apparently peaking before the *Fermi* band and rapidly falling off in the high-energy range. The two upper limits shown are thus upper limits for both the blazar emission and the expected hard, steady component from IC/CMB, with the 3–10 GeV limit being the most constraining.

3. IC/CMB FOR KNOT A IS RULED OUT

In the IC/CMB model, the GeV emission is predetermined by the requirement that IC/CMB emission gives the observed X-ray flux. Consider the synchrotron SED of knot A (Figure 2). The synchrotron emitting electrons will unavoidably produce an IC/CMB component (G06) identical to the synchrotron one but with a shift in peak frequency:

$$\frac{\nu_c}{\nu_s} = \frac{2\pi m_e c(1+z)\nu_0}{e(B/\delta)} = 6.6\times10^4\frac{\delta}{B/B_0} = 6.6\times10^8\ \delta^2, \quad (1)$$

and a shift in peak luminosity:

$$\frac{L_c}{L_s} = \frac{32\pi U_0(1+z)^4}{3(B/\delta)^2} = 2.5\times10^{-11}\left(\frac{\delta}{B/B_0}\right)^2 = 2.5\times10^{-3}\ \delta^4, \quad (2)$$

where ν_c and ν_s are the peak IC and synchrotron frequencies, L_c and L_s are the peak IC and synchrotron luminosities, e and m_e are the electron charge and mass, $B_0 = 1$ G, B is the magnetic field in Gauss, $\nu_0 = 1.6\times10^{11}$ Hz and $U_0 = 4.2\times10^{-13}$ erg cm^{-3} are the CMB peak frequency and energy density at $z = 0$, δ is the Doppler factor, and the last part of each equation holds for equipartition conditions ($B\delta = 10^{-4}$ G; Jester et al. 2005).

To reproduce the UV–X-ray observations of knot A, a $B/\delta = 5.5\times10^{-7}$ G is required ($\delta_{eq} = 13.4$ assuming equipartition). This determines, from the above equations and without any freedom, an IC/CMB component peaking at $\sim10^{24.6}$ Hz with $\sim\nu f_\nu = 10^{-11.7}$ erg s^{-1} cm^{-2}. To demonstrate this, we plot in Figure 2 a numerically calculated SED taking into account electron energy losses and the full Klein–Nishina cross-section. Although this SED corresponds to equipartition conditions, numerical SEDs away from equipartition are practically identical for the required $B/\delta = 5.5\times10^{-7}$ G. The level of the IC/CMB emission at GeV energies violates the upper limit of the 3–10 GeV band at the 99.9% level (Figure 2), *ruling out the IC/CMB interpretation for the X-ray emission of knot A in 3C 273*. This is the main result of this work.

Abandoning the requirement that the UV–X-ray emission of knot A is IC/CMB, we constrain $B/\delta > 1.3\times10^{-6}$ G, or $\delta_{eq} < 9$ from the requirement that the IC/CMB emission from knot A (broken line SED in Figure 2), does not overproduce the 3–10 GeV 95% flux limit.

3.1. Constraints from Knots A through D1

Radio polarization maps (Conway et al. 1993) show that the jet magnetic field runs roughly parallel to the jet from knot A all the way to knot D1. Beyond knot D1 the magnetic field turns abruptly to become orthogonal to the jet axis, as one would expect from a shock that decelerates the flow, and compresses the plasma. The polarization is suggestive of a jet that does not decelerate substantially from knot A to knot D1, but decelerates efficiently past knot D1. It is thus plausible that the flow from knot A to D1 is characterized by a single Doppler factor, and that the magnetic field does not vary significantly, as suggested by the fact that the equipartition magnetic field of all knots is the same within a factor <2 (Jester et al. 2005).

Based on the assumption that a single Doppler factor and magnetic field describe the jet from knot A to D1, we can impose further constraints. In Figure 3 we plot the SED of the total flux from knot A to D1, along with our *Fermi* constraints. As can be seen, to satisfy the 95% 3–10 GeV band *Fermi* limit we require $B/\delta > 4.0\times10^{-6}$ G, or, assuming equipartition, $\delta_{eq} < 5$. The existing shallow TeV limits (3.9 hr of HESS observations, no de-absorption applied; Aharonian et al. 2005) do not provide

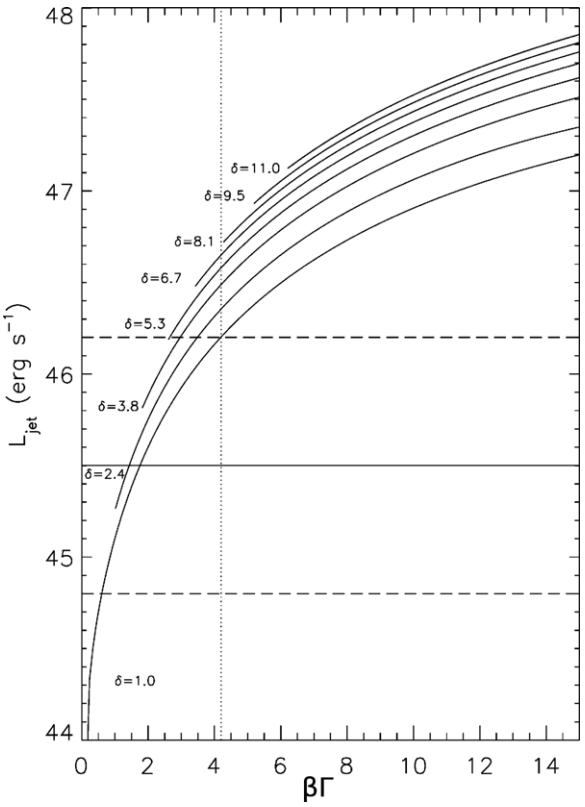

Figure 4. $L_{\rm jet,min}$ as a function of $\beta\Gamma$ for a range of δ. The solid and broken horizontal lines represent the jet power estimate of $L_{\rm jet} = 10^{45.5\pm0.7}$ erg s^{-1} from the X-ray cavity scaling. Jet configurations with $L_{\rm jet,min} > 10^{46.2}$ erg s^{-1} are disfavored, leading to an upper limit of $\Gamma \lesssim 4.2$ for the jet.

useful constraints, but future TeV observations with the planned Cherenkov TeV Array may be able to detect this component.

4. AN UPPER LIMIT ON THE BULK LORENTZ FACTOR

We present here a model-dependent upper limit on Γ, based on an estimate of the jet power $L_{\rm jet} = 10^{45.5\pm0.7}$ erg s^{-1} (Meyer et al. 2011) of 3C 273, derived from the scaling relation between kinetic jet power estimated by the X-ray cavity method and the low-frequency radio lobe emission (Cavagnolo et al. 2010; see also Godfrey & Shabala 2013 for a different method extending the scaling to powerful jets). Assuming that the entire radio to X-ray emission of knot A comes from the same region, the only frequency where an electron cooling break can be manifested is either at $\nu_c = 10^{13.5}$ Hz or $\nu_c \gtrsim 10^{18}$ Hz, given that no break is observed between the UV and X-ray observations (assumed to come from a second synchrotron component).

In the first case, the optical to X-ray emitting electrons are cooled, requiring an electron injection $q_{\rm inj}(\gamma) \propto \gamma^{-1.5}$. To calculate the minimum jet power $L_{\rm jet,min}$ corresponding to a given δ we calculate for a range of Γ the magnetic field B required for $\nu_c = 10^{13.5}$ Hz. The Poynting power is then $L_B = \pi c R^2 \beta \Gamma^2 B^2/(8\pi)$, where R is the radius of knot A. For this B we then calculate the lepton power L_e required to produce the observed SED. With these, $L_{\rm jet,min} = L_B + L_e$, because we do not include protons or thermal electrons. In Figure 4, we show curves of $L_{\rm jet,min}$ as a function of $\beta\Gamma$ for a range of δ Configurations that require $L_{\rm jet,min} > 10^{46.2}$ erg s^{-1} are disfavored, leading to $\Gamma \approx \beta\Gamma < 4.2$.

In the second case the optical to X-ray emitting electrons escape the emission region before cooling and electron injection is steeper, $n_{\rm inj}(\gamma) \propto \gamma^{-2.5}$. This second case of no cooling up to 10^{18} Hz requires that a region significantly smaller than the optical jet lateral size (~1 kpc) is responsible for the UV to the X-ray emission: for example, for $\delta = \Gamma = 5$ the maximum size of this emitting region is ~100 pc, corresponding to a variability timescale of ~70 yr.

5. DISCUSSION

Using upper limits to the *Fermi* flux of the LSJ of 3C 273, we rule out IC/CMB being the X-ray emission mechanism of knot A, the X-ray dominant knot of the LSJ. This result does not depend on any assumptions of equipartition or jet content and is, therefore, robust. Assuming equipartition and a steady flow from knot A to knot D1, as suggested by observations, we set an upper limit to the jet Doppler factor, $\delta \leqslant 5$. Finally, adopting an upper limit to the jet power derived from the X-ray cavity scaling, we find $\Gamma \lesssim 4.2$. We note that the IC/CMB mechanism for the rest of the knots, all downstream of knot A, has been discounted on spectral (X-ray spectrum significantly steeper than the radio) or morphological (radio and optical emission not co-located) grounds (Jester et al. 2005, 2006, 2007).

Our result leaves as the only alternative a synchrotron nature for the X-ray emission. This means that in situ particle acceleration takes place that accelerates electrons at least up to ~30–100 TeV. It is not clear what particle acceleration mechanism produces this second EED. If we assume that this population cools before it escapes the emission region, a very hard electron injection is required ($n_{\rm inj}(\gamma) \propto \gamma^{-1.5}$). On the other hand, if the electrons escape the emission region uncooled, a steeper electron injection is needed ($n_{\rm inj}(\gamma) \propto \gamma^{-2.5}$), but this requires that the emission region is significantly smaller than 1 kpc. Assuming $\delta = \Gamma = 5$ this corresponds to 100 pc and to a variability timescale of ~70 yr (note that X-ray variability with a timescale of a few years has been observed for a kpc scale knot in the LSJ of Pictor A; Marshall et al. 2010). We finally note that while IC/CMB appears to be ruled out in 3C 273, it is possible that other powerful LSJs produce X-rays through IC/CMB.

E.M. acknowledges support from *Fermi* grant NNX13AO88G. M.G. acknowledges support from *Fermi* grant NNX12AF01G.

REFERENCES

Aharonian, F., Akhperjanian, A. G., Bazer-Bachi, A. R., et al. 2005, A&A, 441, 465
Barndorff-Nielwson, O. E., & Cox, D. R. 1994, Inference and Asymptotics (London: Chapman and Hall)
Cara, M., Perlman, E. S., Uchiyama, Y., et al. 2013, ApJ, 773, 186
Cavagnolo, K. W., McNamara, B. R., Nulsen, P. E. J., et al. 2010, ApJ, 720, 1066
Celotti, A., Ghisellini, G., & Chiaberge, M. 2001, MNRAS, 321, L1
Chartas, G., Worrall, D. M., Birkinshaw, M., et al. 2000, ApJ, 542, 655
Conway, R. G., Garrington, S. T., Perley, R. A., & Biretta, J. A. 1993, A&A, 267, 347
Dermer, C. D., & Atoyan, A. 2004, ApJL, 611, L9
Fanaroff, B. L., & Riley, J. M. 1974, MNRAS, 167, 31P
Georganopoulos, M., Perlman, E. S., Kazanas, D., & McEnery, J. 2006, ApJL, 653, L5 [G06]
Godfrey, L. E. H., & Shabala, S. S. 2013, ApJ, 767, 12
Hardcastle, M. J. 2006, MNRAS, 366, 1465
Hardcastle, M. J., Worrall, D. M., Birkinshaw, M., Laing, R. A., & Bridle, A. H. 2002, MNRAS, 334, 182
Harris, D. E., & Krawczynski, H. 2006, ARA&A, 44, 463
Jester, S., Harris, D. E., Marshall, H. L., & Meisenheimer, K. 2006, ApJ, 648, 900
Jester, S., Meisenheimer, K., Martel, A. R., Perlman, E. S., & Sparks, W. B. 2007, MNRAS, 380, 828

Jester, S., Röser, H.-J., Meisenheimer, K., & Perley, R. 2005, A&A, 431, 477
Jorstad, S. G., & Marscher, A. P. 2004, ApJ, 614, 615
Marshall, H. L., Hardcastle, M. J., Birkinshaw, M., et al. 2010, ApJL, 714, L213
Mehta, K. T., Georganopoulos, M., Perlman, E. S., Padgett, C. A., & Chartas, G. 2009, ApJ, 690, 1706
Meyer, E. T., Fossati, G., Georganopoulos, M., & Lister, M. L. 2011, ApJ, 740, 98
Nolan, P. L., Abdo, A. A., Ackermann, M., et al. 2012, ApJS, 199, 31
Perlman, E. S., & Wilson, A. S. 2005, ApJ, 627, 140
Sambruna, R. M., Donato, D., Cheung, C. C., Tavecchio, F., & Maraschi, L. 2008, ApJ, 684, 862
Sambruna, R. M., Gambill, J. K., Maraschi, L., et al. 2004, ApJ, 608, 698
Sambruna, R. M., Urry, C. M., Tavecchio, F., et al. 2001, ApJL, 549, L161
Schwartz, D. A., Marshall, H. L., Lovell, J. E. J., et al. 2000, ApJL, 540, L69
Siemiginowska, A., Stawarz, Ł., Cheung, C. C., et al. 2007, ApJ, 657, 145
Tavecchio, F., Maraschi, L., Sambruna, R. M., & Urry, C. M. 2000, ApJL, 544, L23
Uchiyama, Y., Urry, C. M., Cheung, C. C., et al. 2006, ApJ, 648, 910
Wilson, A. S., & Yang, Y. 2002, ApJ, 568, 133
Worrall, D. M. 2009, AA&Rv, 17, 1
Worrall, D. M., Birkinshaw, M., & Hardcastle, M. J. 2001, MNRAS, 326, L7